

pubs.acs.org/JACS Article

Engineering Metastability into a Virus-like Particle to Enable Triggered Dissociation

Caleb A. Starr, Smita Nair, Sheng-Yuan Huang, Michael F. Hagan, Stephen C. Jacobson, and Adam Zlotnick*



Cite This: J. Am. Chem. Soc. 2023, 145, 2322-2331



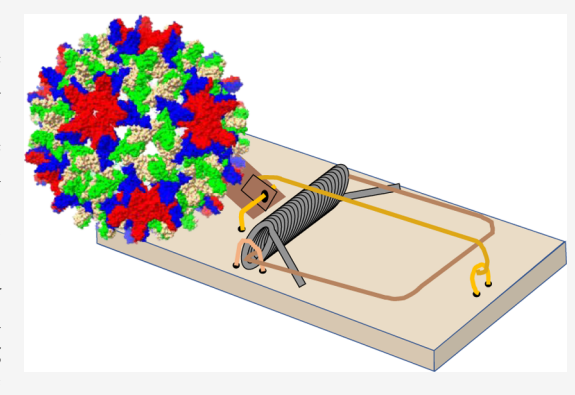
ACCESS

III Metrics & More

Article Recommendations

Supporting Information

ABSTRACT: For a virus-like particle (VLP) to serve as a delivery platform, the VLP must be able to release its cargo in response to a trigger. Here, we use a chemical biology approach to destabilize a self-assembling capsid for a subsequent triggered disassembly. We redesigned the dimeric hepatitis B virus (HBV) capsid protein (Cp) with two differentially addressable cysteines, C150 for reversibly crosslinking the capsid and C124 to react with a destabilizing moiety. The resulting construct, Cp150-V124C, assembles into icosahedral, 120-dimer VLPs that spontaneously crosslink via the C-terminal C150, leaving C124 buried at a dimer—dimer interface. The VLP is driven into a metastable state when C124 is reacted with the bulky fluorophore, maleimidyl BoDIPY-FL. The resulting VLP is stable until exposed to modest, physiologically relevant concentrations of reducing agent. We observe dissociation with FRET relaxation of polarization, size



exclusion chromatography, and resistive-pulse sensing. Dissociation is slow, minutes to hours, with a characteristic lag phase. Mathematical modeling based on the presence of a nucleation step predicts disassembly dynamics that are consistent with experimental observations. VLPs transfected into hepatoma cells show similar dissociation behavior. These results suggest a generalizable strategy for designing a VLP that can release its contents in an environmentally responsive reaction.

■ INTRODUCTION

Capsids of simple viruses self-assemble to package their genomes at one end of their life cycle and dissociate to release their genomes at the other end. In medicine and nanotechnology, virus-like particles (VLPs), the capsids without a genome, have seen many uses including as platforms for antigen display, ^{1–8} as drivers of oncolysis, ^{9–11} and as containers for enzymes, nanoparticles, and small molecules. ^{9,12–20} While there are many ways of packaging materials in a VLP, releasing the contents of the particle in a programmed manner remains a barrier, the goal of the following study.

The hepatitis B virus (HBV) capsid (or core) protein (Cp) has figured prominently as an epitope platform for vaccination, ^{2,4,21,22} as a model system for self-assembly, ^{23–28} and as a target for assembly-directed HBV antiviral agents. ^{29–33} HBV assembly studies have focused on the Cp assembly domain (Cp149), a 149-residue, all-helix protein that forms an obligate homodimer and can be induced to assemble into a capsid by high ionic strength (Figure 1). ³⁴ Assembly reactions are characterized by weak subunit—subunit interactions which at -3.5 kcal mol⁻¹ contact⁻¹ are able to support assembly because each dimer makes four contacts. Assembly reactions have a complex nucleation phase followed by association of one dimer at a time to form an icosahedral

capsid. ^{25–28} Few intermediates ever accumulate. The resulting capsids are a mixture of T=4, 120-dimer particles and T=3, 90-dimer particles, with the T=4 form being predominant. The interdimer surface contacts in capsids are about 1200 Ų each and largely hydrophobic. While assembly is based on weak interactions, assembled capsids are surprisingly persistent. ^{24,35} In vivo, capsid dissociation involves biological cues and may be driven by the internal pressure of packaged nucleic acid. ^{36,37}

Assembly-directed antivirals against HBV take advantage of both assembly and disassembly. These molecules are being developed in the search for a cure to endemic chronic HBV, which infects almost 300 million people and leads to about 800,000 deaths each year. Assembly-directed molecules (known as capsid assembly modulators or capsid protein allosteric modulators, CAMs or CpAMs) bind to a pocket at the interdimer interface. They promote assembly by increasing the amount of buried nonpolar surface area. Because

Received: October 15, 2022 Published: January 18, 2023





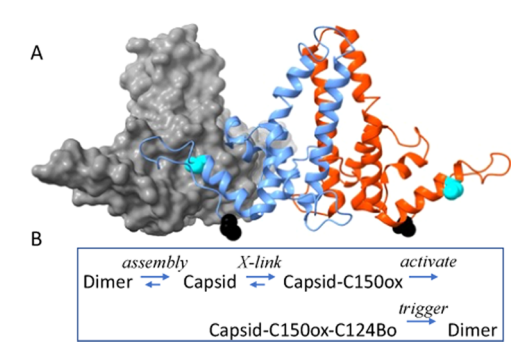


Figure 1. Workflow for stabilization and dissociation of Cp150-V124C capsids. (A) Dimer of Cp150-V124C dimers. The front dimer (blue and red) shows the position of residue 124 (cyan), which is buried at the interface with the surface-shaded dimer and the C-terminus of the molecular model (black), which indicates the localization of C150. (B) In our workflow, Cp150-V124C dimers are assembled into 120-dimer capsids. Capsids become crosslinked by C150-C150 disulfides. Capsids are activated by the reaction of C124, buried at interdimer interfaces, with maleimidyl-BoDIPY FL. The resulting metastable capsids are triggered to dissociate by reducing agents such as β ME.

they are a molecular wedge at the dimer interface, CAMs lead to capsid expansion and distortion. If the distortion is great enough, the CAM can lead to capsid disruption. 44,30,38

The abilities of HBV Cp to self-assemble and to carry decorations that may direct the assembled VLP to specific cells make this system an attractive platform for delivering large and small molecules to the target. However, VLP resistance to dissociation limits its utility for delivering its cargo. We have taken a chemical biology strategy to develop triggered disassembly: assemble a capsid, crosslink this capsid through disulfide bonds, chemically modify the CAM binding pocket to destabilize the capsid, and then demonstrate that reducing the crosslinks under physiologically relevant conditions and in cells allows the capsid to dissociate.

MATERIALS AND METHODS

Mutagenesis, Cloning, and Purification of Cp150-V124C. The V124C mutation was incorporated into the pET11c vector expressing Cp150 with Quikchange Mutagenesis (Stratagene). The oligos for mutagenesis were:

sense - 5'-gaggagtgcgaatccaacatccaaaagacaccaaatactctagaaccgt-3'. antisense - 5'-acggttctagagtatttggtgtcttttggatgtggattcgcactcctc-3'.

Mutation was confirmed by Sanger sequencing (Eurofins Genomics). The new plasmid was transformed into a BL21(DE3) *Escherichia coli* overexpression system. Cp150-V124C dimer was expressed and purified as previously described. ⁴⁵ Dimer concentrations were determined with an ε_{280} of 60,900 cm⁻¹.

VLP Assembly and BoDIPY-FL Modification. Cp150 and Cp150-V124C dimers were assembled by buffer exchanging the protein from the storage buffer to 50 mM 4-(2-hydroxyethyl)-1-piperazineethanesulfonic acid (HEPES), pH 7.5, mixing the required proportion of the two proteins, adjusting the final concentrations to 25 μ M dimer in 300 mM NaCl, 50 mM HEPES pH 7.5 (assembly buffer), and allowing the reaction to equilibrate for 24 h at 25 °C. Assembled VLPs were isolated from free dimer by size exclusion chromatography (SEC) using a Superose-6 Increase 30/100 column (Cytiva Lifesciences) equilibrated in assembly buffer. VLPs were allowed to sit at room temperature until fully oxidized following the protocol of Lee et al. 46 Oxidation was confirmed by nonreducing sodium dodecyl sulfate poly(acrylamide) gel electrophoresis (SDS-PAGE), showing almost exclusively dimeric protein (Supporting Figure 1). Quantitative disulfide crosslinking ensured that the

majority of cysteines available for modification in the VLPs were C124s.

For maleimidyl-BoDIPY-FL labeling, VLPs were diluted to 15–20 μ M, then a 10-fold molar excess of maleimidyl-BoDIPY-FL was added. After 24 h at 4 °C, excess label was removed either (i) by mixing with activated charcoal (50 mg mL⁻¹) for 10 s and then filtering through a 0.22 μ m filter or (ii) by buffer exchanging the reaction with a PD10 desalting column (Cytiva Lifesciences) to 300 mM NaCl, 50 mM HEPES pH 7.5. The ratio of BoDIPY-FL to dimer was determined by the relative absorbance of dye and protein. Typical labeling efficiency for these reactions is 80–90%. The state of the series of the

SEC of VLP Dissociation Reactions. For control reactions, Cp150-V124C VLPs were diluted to 5 μ M and incubated with 3 M urea or 3 M urea and 50 mM dithiothreitol (DTT) for 24 h. After 24 h, the reactions were resolved by injecting onto a 21 mL Superose-6 column (GE) equilibrated in 300 mM NaCl, 50 mM HEPES pH 7.5, that was plumbed to a Shimadzu HPLC equipped with a diode array absorbance detector (Shimadzu).

For beta mercaptoethanol (β ME)-induced dissociation experiments, VLPs were diluted to 5 μ M and incubated with the appropriate β ME concentrations. Reactions were carried out in 150, 300, or 500 mM NaCl in 50 mM HEPES pH 7.5. After the addition of β ME, reactions were equilibrated for 2 h before injecting onto a 21 mL Superose-6 column (GE) equilibrated with 150, 300, or 500 mM NaCl depending on which set of reactions was being measured. Peaks in the chromatograms at 280 nm absorbance were integrated over the capsid and dimer elution volumes to determine the relative fraction of capsids and dimers in each reaction.

Fluorescence Polarization (FP) of Cp150-V124CBo VLP Dissociation. Purified VLPs were diluted into the appropriate buffer in a Greiner 96-well black, flat-bottom, Fluotrac plate. β ME in assembly buffer was added to the selected final concentration and then loaded into a Neo2 plate reader (BioTek, Winooski, VT) with a filter cube equipped with polarizers. The FP of the samples was observed once per minute for 2 h.

Resistive-Pulse Sensing. The nanofluidic devices were designed with two V-shaped microchannels connected by four nanopores in series for resistive-pulse measurements. ^{25,48} The nanopores were 50 nm deep, 50 nm wide, and 300 nm long, and nanochannels between the nanopores were 100 nm deep, 300 nm wide, and 500 nm long. For dissociation reactions, capsids assembled from 10 μ M Cp150-V124CBo dimer in 50 mM HEPES pH 7.5 with 300 mM NaCl were reacted with 0, 20, 50, and 100 mM β ME for 120 min, and then the reactions were quenched by diluting to a final concentration of 0.1 μ M dimer, 50 mM HEPES pH 7.5 with 500 mM NaCl for resistive-pulse measurements. The reaction mixture was placed in the sample reservoir and drawn through the nanofluidic device electrophoretically. Detailed descriptions of the resistive-pulse measurements and data analysis are in the Supporting Information.

Computational Modeling. We modeled the triggered disassembly process with a simplified rate equation description. We assume that the process starts at time t=0 from capsids that are completely assembled and fully crosslinked. Here, we have assumed that the capsid has 100% Cp150-V124C. Dissociation is considered to be sensitive to the size of the cluster of crosslinks that must be broken for a subunit to be released, n, where n is essentially a Hill coefficient. Nucleation occurs at a rate $k_{\rm nuc}$ and the rate of crosslink cleavage is $k_{\rm ul}$. The rate of crosslink cleavage is considered to be proportional to the reducing agent concentration. We denote the fraction of subunits in capsids as $f_{\rm cap}$ and the fraction of non-crosslinked subunits in assembled capsids as $f_{\rm ul}$. Taking this mean field approach, the resulting rate equation

$$\frac{\mathrm{d}f_{\mathrm{cap}}}{\mathrm{d}t} = -k_{\mathrm{nuc}}(1 - f_{\mathrm{ul}})^{n} f_{\mathrm{cap}} \tag{1}$$

is numerically integrated over time and reported in nondimensional time $k_{\rm nuc}t$. A detailed description of the model is available in the Supporting Information.

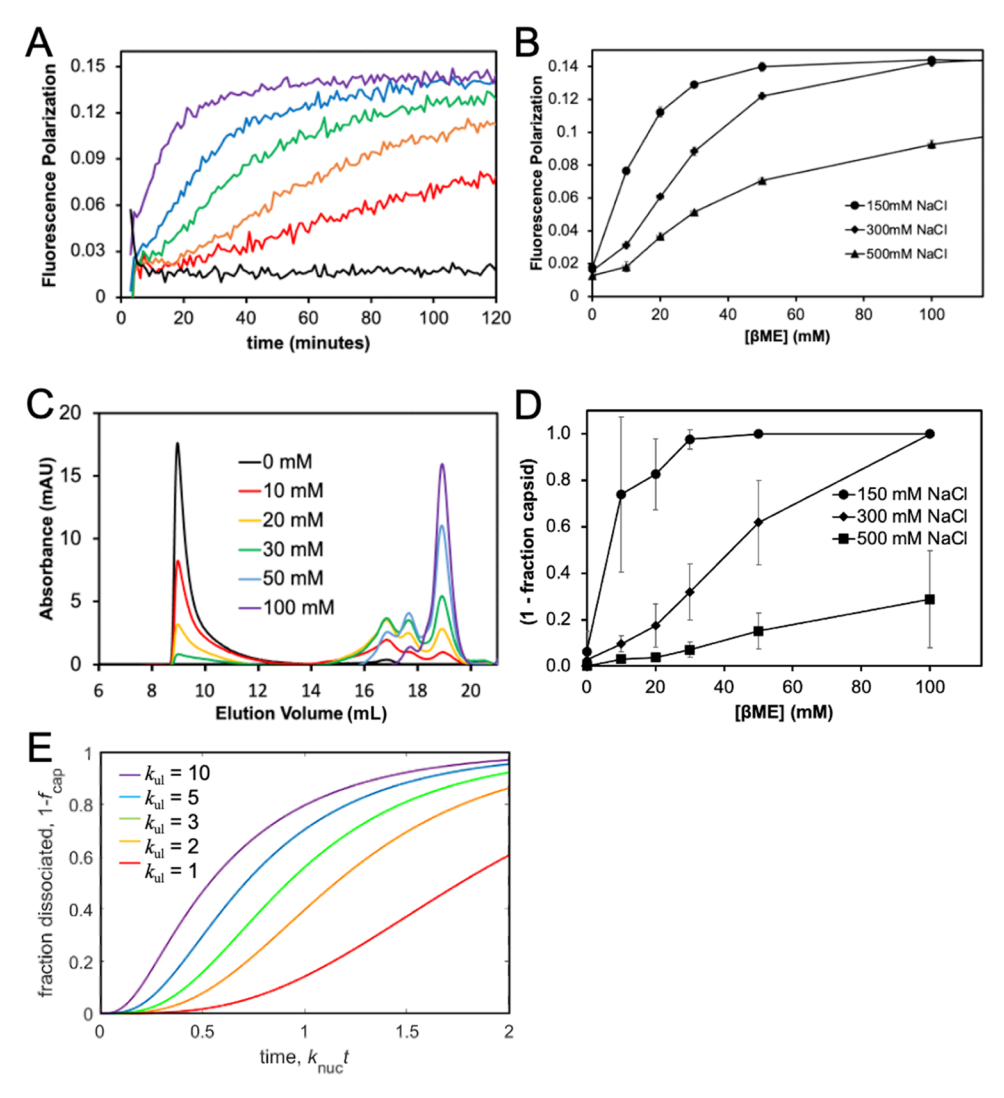


Figure 2. Kinetics of Cp150-V124CBo capsid dissociation. (A-D) Cp150-V124CBo capsids (5 \(\mu \) M dimer) in 150, 300, or 500 mM NaCl were mixed with varying β ME concentrations. (A) Reactions in 150 mM NaCl were observed by fluorescence polarization (FP) for 120'. β ME concentrations use the color key shown in (C). (B) FP at 120' shows that capsid stabilizing NaCl inhibits dissociation. Notably, the capsids in 500 mM NaCl are not fully dissociated. (C) In parallel experiments, samples in 150 mM NaCl were incubated for 120' with varying β ME, and then, reactions were resolved by size exclusion chromatography (SEC) to show the remaining capsid, dimer, and intermediates. (D) Dissociation determined by SEC, in terms of the remaining capsid, reveals a similar pattern of sensitivity to ionic strength and reducing potential as the FP experiments. In higher ionic strength, capsids appear to be slightly more persistent by SEC than by FP. (E) Simulations of capsid dissociation kinetics show a sensitivity to the rate of crosslink breaking (k_{nl}) that approximately parallels the FP kinetics observed in (A). For this calculation, at least three crosslinks near a leaving subunit had to be broken for a subunit to leave. Further details are shown in Supporting Data.

Cell Culture, Protein Transfection, and Fluorescence Microscopy. HuH7-H1 cells were maintained in DMEM-F12 (Gibco) media supplemented with 5% fetal bovine serum (FBS) (Gibco), 1 × penicillin–streptomycin (Sigma), 600 μ g mL⁻¹ of G418 (Clontech) at 37 °C and 5% CO₂. Protein transfections were performed with 50 ng of capsid protein with the Xfect Protein Transfection kit (Clontech) according to the manufacturer's protocol. After transfection, the cells were incubated for 4 h at 37 °C, washed with phosphate-buffered saline (PBS), fixed with 4% paraformaldehyde, and permeabilized with 0.2% Triton X-100 before labeling with a 1:500 dilution of the Mab3120 monoclonal anti-Cp antibodies (Institute of Immunology Co., Ltd.), and then probed with a 1:500 dilution of AlexaFluor594-conjugated goat anti-mouse secondary antibody (Thermo Fisher Scientific). The cells were visualized with a Leica TCS SP8 confocal microscope equipped with Leica HyD Detector, a 63× (f1.4 numerical aperture) oil immersion objective, and appropriate lasers for exciting DAPI, BoDIPY, and Alexa-Fluor594. A detailed description of transfection and sample preparation is available in the Supporting Information.

Protein Blot. For western analysis, 50, 100, 200, and 500 ng of Cp150-V124C and Cp150-V124C-Bo capsid were blotted onto Immobilon-P transfer membrane (Millipore). The blots were blocked with 5% skim milk in PBS and probed with a 1:500 dilution of Mab3120 monoclonal anti-Cp antibodies (Institute of Immunology Co., Ltd.) for 2 h at room temperature followed by washing with 1 × PBS-T (PBS with 0.1% Tween-20) and $1 \times$ PBS. The blot was then probed with a 1:15,000 dilution of IRDye 600LT goat anti-mouse secondary antibodies (LI-COR) for 1 h. The blots were washed with 1 × PBS-T and imaged on a ChemiDoc MP imaging system (Bio-Rad).

RESULTS

Our underlying goal was to design a capsid that would be stable until triggered to dissociate by a biologically compatible signal. Toward this end, we introduced a V124C mutation into Cp150 (Cp149-V48A, C61A, C107A, C150). In Cp150, all native cysteines of HBV core protein are mutated to alanine

and a C-terminal cysteine is appended. Cp150 readily crosslinks after assembly resulting in a highly stable capsid.⁴ The V124C mutation in a Cp149-3CA (all native cysteines mutated to alanine) has little effect on capsid assembly but induces dissociation when reacted with maleimidyl-BoDIPY. 49 The combination, Cp150-V124C, thus has two accessible cysteines: one on helix 5 (the C-terminal helix), which is the small molecule binding pocket and one at the C-terminus (Figure 1A). We expected the construct to be a stable homodimer that assembles in response to increased ionic strength, would be stabilized by oxidation of C150-C150 disulfide bonds, would be driven to a metastable state by reaction of C124 with maleimidyl-BoDIPY FL, and could be relaxed to a lower energy state by disulfide reduction to dissociate the capsid and release dimeric Cp150-V124CBo (Figure 1B).

Cp150-V124C dimer was expressed and purified from *E. coli* with a yield of 150 mg from 2 L of TB broth. As with other Cp149 and Cp150 constructs, Cp150-V124C was initially isolated as a capsid that was dissociated to dimer by nondenaturing concentrations of urea (3 M) under reducing conditions. The Cp150-V124C readily reassembled in response to 300 mM NaCl; these VLPs were isolated by SEC, leaving behind an $\sim 6~\mu M$ dimer, the pseudo-critical concentration of assembly. Isolated capsids, after air oxidation (Supporting Figure 1), were stable in 3 M urea (Supporting Figure 2). Once assembled and oxidized, capsids were treated with maleimidyl BoDIPY-FL. Based on absorbance, we achieved $\sim 80\%$ labeling.

We hypothesized that BoDIPY modification of C124 would destabilize the protein-protein interaction, leaving the capsid held together by disulfides. To test this hypothesis, capsids were treated with a reducing agent, β ME, and dissociation was monitored by changes in BoDIPY fluorescence polarization (FP). In this assay, we take advantage of a seemingly paradoxical near-zero FP of assembled capsid due to self-FRET.⁵⁰ Each capsid has upward of 200 BoDIPY adducts bound to V124C. The BoDIPY-BoDIPY Förster distance is 5.7 nm, and the average distance between the quasi-equivalent C-alphas of the C124 is about 3.7 nm. Therefore, the BoDIPY adducts are well within the distance for self-FRET. The net result of self-FRET with an array of fluorophores is that energy is transferred from an oriented fluorophore to a randomly oriented fluorophore with a resulting loss of polarization. However, when dissociation occurs and individual dimers are released from the capsid lattice, the two fluorophores bound to a single dimer are at least 6 nm apart, more than the Förster distance, resulting in a larger FP signal for dimer than for

The purified and labeled Cp150-V124CBo capsids were subjected to increasing reducing conditions to test for dissociation. We used beta mercaptoethanol (β ME) instead of DTT due to its milder reducing potential and its single thiol group that mimic the glutathione system (GSH) found in cells. Cp150-V124CBo capsids were incubated with 0, 10, 20, 30, 50, 100, 150, 200, and 250 mM β ME, and the FP signal was measured every minute for 2 h. We also examined the effect of residual protein—protein interaction by examining dissociation in different ionic strengths (Figure 2 and Supporting Figure 3).

Once β ME was added to Cp150-V124CBo capsids, even at the lowest tested concentration of 10 mM, the FP signal began to increase, indicating dissociation. In control experiments without β ME, there was no change in the FP. Dissociation

kinetics were sigmoidal and relatively slow, taking on the order of minutes to hours to equilibrate.

Dissociation kinetics were dependent upon reducing potential and capsid stability. As the β ME concentration increased up to 100 mM, so did the rate of dissociation. Increasing the ionic strength stabilizes capsids, by favoring an assembly-active state and/or by suppressing electrostatic repulsion between subunits, $^{51-53}$ and also resulted in less dissociation and slower kinetics (Figure 2A and Supporting Figure 3A–C). Viewed at a time point of 2 h (Figure 2B and Supporting Figure 3D), dissociation in the 150 mM NaCl reactions flattens out by 50 mM β ME, indicating complete dissociation. In 300 mM NaCl, complete dissociation was shifted slightly to 100 mM β ME. Notably, in 500 mM NaCl dissociation is incomplete even at 250 mM β ME (Supporting Figure 3C,D). In summary, BoDIPY labeling of Cp150-V124C capsids destabilized and primed them for triggered dissociation.

The FP dissociation assay was consistent with a complementary test of dissociation by SEC. SEC has the advantage of precisely quantifying the components of a reaction but lacks temporal resolution. In these studies, the VLP was incubated for 2 h with a range of β ME concentrations and 150, 300, or 500 mM NaCl (Figure 2D and Supporting Figure 4). When no β ME was present, there was a large capsid peak with a very small dimer peak.

Adding any amount of β ME to the capsids resulted in measurable dissociation as evidenced by a decrease in the capsid peak area and a concomitant increase in the dimer peak area. At 150 mM NaCl (Figure 2C), dissociation was nearly complete by 30 mM β ME, measured by the loss of the capsid peak. However, especially at low β ME, small oligomers of dimer were also seen. At 300 mM NaCl (Figure 2D and Supporting Figure 4B,D), dissociation was not complete until 100 mM β ME. In 500 mM NaCl (Supporting Figure 4C,D), dissociation was attenuated; at 100 mM, β ME only 30% of capsids dissociated (Figure 2D). The SEC results agreed qualitatively with the FP assay, confirming that Cp150-V124CBo capsids were, in fact, dissociating. There is a systematic difference, however, with the SEC results consistently showing less dissociation than FP (Figure 2B,D). Part of this difference may arise from capsids with missing subunits, where BoDIPY dyes are not within FRET distance of neighbors and, thus, give a signal for dissociation though they are part of a complex. Another source of difference is that capsids lacking a few subunits will comigrate with intact particles in SEC.

We examined dissociation at the single particle level with nanofluidic resistive-pulse sensing (RPS) (Figure 3). In RPS, changes in the current of a nanofluidic circuit are measured as particles are electrophoretically driven through nanopores, displacing conductive electrolyte. The amplitude of each current pulse is proportional to the volume of electrolyte displaced, which, in turn, is proportional to the particle size. In addition to monitoring dissociation, resistive-pulse measurements were used to confirm the particle sizes (Supporting Figure 5) and surface charge densities (Supporting Figure 6). Capsids assembled from Cp149, Cp150-V124C, and Cp150-V124C-Bo were similar and did not change with particle modification. RPS has been a powerful tool to examine the assembly and dissociation of HBV VLPs. S4-56

For these experiments, we examined dissociation reactions in 300 mM NaCl as a function of β ME concentration. These

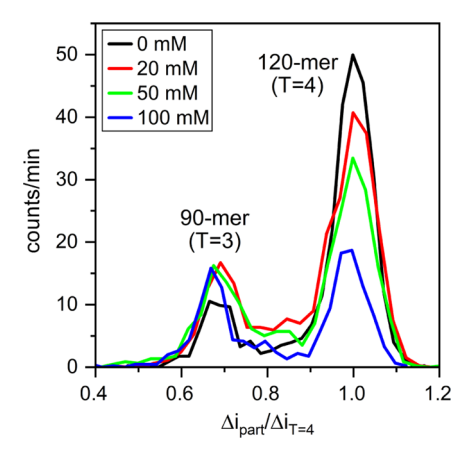
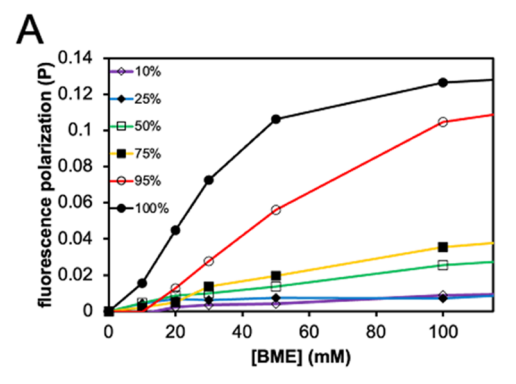


Figure 3. Single-molecule observations of Cp150-V124C-Bo dissociation shows loss of T=4 capsids. Cp150-V124CBo VLPs were subjected to increasing amounts of β ME (0, 20, 50, and 100 mM) in 300 mM NaCl, and the distributions of products were measured by nanofluidic resistive-pulse sensing (RPS) after incubating samples in β ME for 120 min and then diluting the samples 100-fold, effectively stopping the dissociation reaction. The rightmost peaks in these histograms correspond to 120-dimer T=4 particles; the leftmost peaks correspond to 90-dimer particles, including T=3 particles. The particle size $(\Delta i_{T=4})$.

reactions were effectively quenched by diluting them 100-fold to a final concentration of 0.1 μM dimer in 50 mM HEPES with 500 mM NaCl for resistive-pulse measurements. The higher ionic strength gave a strong signal in RPS and facilitated capturing reactions that had not equilibrated. Typical for RPS studies of HBV, we observed 120-dimer (T = 4) and 90-dimer (T = 3) capsids in control experiments. As the concentration of β ME increased, counts/min for T = 4 capsids decreased, particles intermediate between T = 4 capsids and 90-mers increased, and the 90-mer counts/min stayed constant. These observations are consistent with a capsid dissociating by the loss of one dimer (or a small cluster of dimers) at a time, ⁵⁶ which contributed to developing a model of triggered dissociation. The persistence of 90-mers may indicate that T = 3 particles are more resistant to dissociation in high ionic strength or that 90-dimer intermediates transiently accumulate. This last possibility is consistent with capsid dissociation passing through a percolation threshold where HBV capsids can persist till about 25% of their subunits are removed, after which they catastrophically fail. 46,56-58

To determine how much BoDIPY labeling was required to destabilize the capsids, we co-assembled Cp150-V124C dimers with Cp150, which lacks C124. We again used FP to examine the kinetics of dissociation. The 120 min timepoints showed that disruption was very sensitive to the fraction of Cp150-V124CBo that was in the capsid (Figure 4). Even at 250 mM β ME, capsids with 75% Cp150-V124C had less than half the FP expected for the release of dimer. With less than 50 mM β ME, only capsids that were 100 and 95% Cp150-V124C showed substantial dissociation.

Again, we used SEC to confirm the results of the FP assay. After incubating co-assembled VLPs with β ME for 2 h, they were analyzed by SEC to determine the amount of capsid and dimer directly (Figure 4B). For these studies, we focused on \leq 100 mM β ME where the 100% Cp150-V124CBo capsids almost fully dissociated. By SEC, as with the FP, it was apparent that the 95% Cp150-V124C sample was very similar



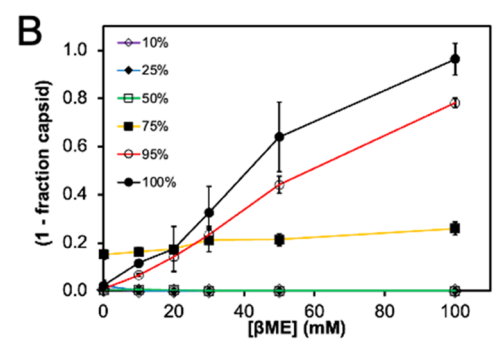


Figure 4. Capsid dissociation is sensitive to the proportion of modified subunit. Capsids were co-assembled with Cp150 and Cp150-V124C and then destabilized with BoDIPY FL. (A) Dissociation characterized by FP of capsids in 300 mM NaCl with varying β ME for 120 min. Capsid stability is inversely proportional to the percentage of Cp150-V124C present during co-assembly. The color code defining the percentage of Cp150-V124C in co-assembly reactions is shown in the figure legend. (B) SEC characterization of these samples largely recapitulated the FP results.

to the 100% Cp150-V124C sample. The 75% Cp150-V124CBo sample showed middling dissociation between the 95 and 50% Cp150-V124C samples. The 50% Cp150-V124C VLPs showed no dissociation by SEC, as did the 25 and 10% samples. Again, FP overestimated the amount of dissociation relative to SEC.

Capsid dissociation kinetics show a lag phase and sensitivity to reducing agent concentration, dimer—dimer association energy, and the fraction of activated dimers. We sought a minimal model to describe the dissociation reaction (Figure 2E, Supporting Figure 7, and Supporting Methods). We reasoned that dissociation of a dimer could require breaking multiple disulfide bonds (n), essentially a Hill coefficient or a nucleus of disrupted interactions, and would be sensitive to the net rate of un-crosslinking ($k_{\rm ul}$), proportional to the concentration of β ME. For this initial calculation, we have used ordinary differential equations and have assumed a uniform distribution of un-crosslinked subunits distributed across all capsids and that all subunits are equal, ignoring the complication of quasi-equivalence.

We observe that changing $k_{\rm ul}$ results in extending the lag phase and slowing the rate of capsid disruption (Figure 2E). In contrast, changing n results in offsetting the dissociation curve with only a modest change in slope. Computationally varying $k_{\rm ul}$ corresponds well with changing the concentration of β ME in our kinetic observations (Figure 2A). There is a similar change in both the rate and lag phase when we experimentally change the association energy between subunits, supporting

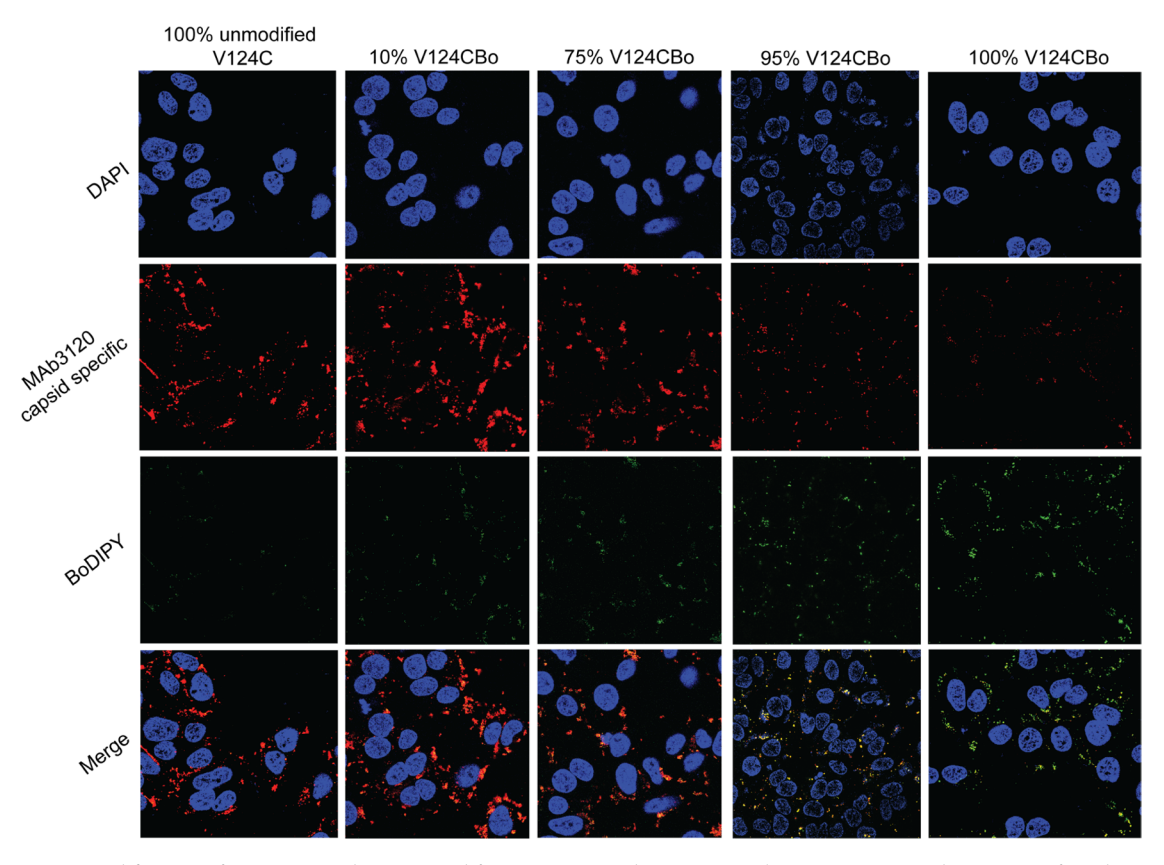


Figure 5. BoDIPY modification of V124C capsids is required for spontaneous dissociation in hepatocytes. Capsids were transfected into HuH7-H1 cells which after 4 h were fixed and probed with a capsid-specific monoclonal antibody and then visualized by epifluorescence microscopy. The first column shows that V124C capsids cluster around nuclei and stain well with MAb3120. Little BoDIPY fluorescence was observed due to no BoDIPY labeling. In the following columns, the transfected samples were of co-assembly reactions of Cp150 with 10, 75, 95, and 100% Cp150-V124C labeled with maleimidyl BoDIPY FL.

the speculation that the rate of un-crosslinking is intrinsically connected to the stability of subunit—subunit interaction.

The ultimate test of the Cp150-V124CBo VLP as a nanocontainer with a redox-sensitive trigger was to test their ability to respond to a reducing cellular environment (Figure 5). Fluorescence confocal microscopy was used to examine HuH7-H1 human hepatoma cells that were transfected with 50 ng of Cp150-V124CBo VLPs and immunostained to differentiate between VLP and dimer. We note that most cell types are estimated to have 1-3 mM glutathione while in hepatocytes glutathione may be as high as 10 mM.⁵⁹ In a control experiment, Cp150-V124C capsids were transfected into cells. These stained strongly with Mab3120, a capsidspecific monoclonal antibody,⁶⁰ and were entirely cytoplasmic. As expected, there was negligible signal for BoDIPY. As the amount of V124CBo in the transfected capsid increased, the amount of signal for BoDIPY (excitation at 494 nm) proportionately increased. However, the signal associated with Mab3120 decreased steeply in the sample with 95% V124CBo and nearly disappeared with 100% V124CBo capsids. In most cases, there was colocalization of the BoDIPY and Mab3120 signals, especially obvious with 75 and 95% Cp150-V124CBo. Even with the 100% Cp150-V124CBo capsids, (i) there were sites where there was colocalization of capsid-specific monoclonal antibody with BoDIPY and (ii) sites where there was only BoDIPY signal. Strikingly, the puncta for the 100% Cp150-V124CBo cells were notably smaller than in samples where there was substantial labeling

with Mab3120, suggesting that capsids in cells may stick together.

We used an immuno dot blot assay to ensure that the MAb3120 antibody would bind to Cp150-V124C and Cp150-V124CBo capsids (Supporting Figure 8). We were concerned because the Mab3120 binding site on capsids is directly above the CAM pocket where the BoDIPY adduct of C124 might distort the Mab3120 epitope. We observed that Mab3120 bound to 75 and 95% Cp150-V124CBo capsids nearly as well as unlabeled capsids. In the 100% Cp1250-V124CBo sample, we saw a significantly weaker signal, which suggests that the antibody may only interact with sites on Cp150-V124CBo that failed to label (typical labeling for these reactions is 80–90%).

These results are consistent with the dissociation of Cp150-V124CBo capsids in a reducing cellular environment. In cells and with isolated complexes, dissociation has the same sensitivity to the fraction of capsid that has disruptive BoDIPY labeling (Figures 4 and 5).

DISCUSSION

A modified HBV Cp was engineered to form a metastable VLP that dissociates in a reducing environment. Essentially, this programmable nanocontainer can release its cargo in response to a reducing cellular environment.

There are two keys to the metastable HBV VLP: the C150-C150 crosslink and the destabilizing V124C mutant. To generalize the destabilizing mutation makes it important to discuss the characteristics of the site. HBV capsid assembly

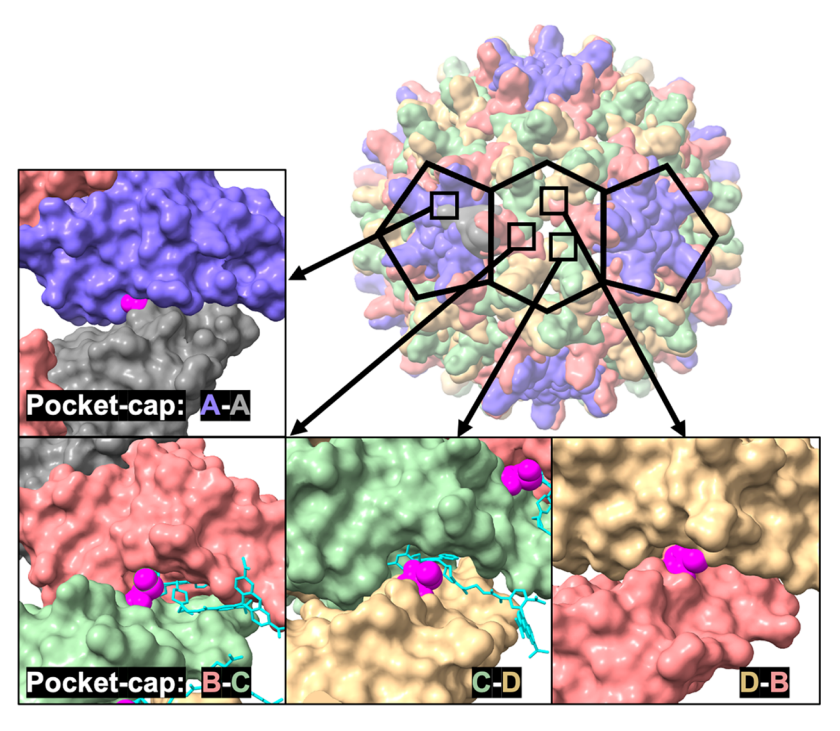


Figure 6. Quasi-equivalent sites have different capacities to fit maleimidyl modification of V124C. A T = 4 HBV capsid (top right) with pentagons and a hexagon outlining selected fivefold and quasi-sixfold vertices. Fivefolds are composed of A subunits (purple, one subunit is gray for contrast). Quasi-sixfolds have true twofold symmetry and a repeat of B, C, and D subunits (red, green, and yellow, respectively). Black squares outline the sites of subunit—subunit interaction that are highlighted with the four insets, which show the accessibility of the CAM sites from the capsid interior. CAM sites in HBV are comprised of a pocket in one subunit that is capped by helix 5, including the V124C mutation, of the adjacent subunit (**Figure 1A**). In this model (based on PDB 6BVF), maleimidyl groups (magenta) are attached to C124 of the capping subunit (bottom); these collide with the A—A and D—B pocket subunits but not the B—C and C—D pocket subunits. B—C and C—D sites are more open and can also accommodate bulky CAMs like HAP-TAMRA (cyan) as seen in the 6BVF structure. Graphics were generated with ChimeraX.

depends on weak interactions, -3.5 kcal mol⁻¹ of contact, between the tetravalent dimer subunits. Contributing to the weakness of the contact is that the buried surface has cavities formed at the interdimer contact.⁴² Pharmacologically, these sites have been targeted by CAM assembly agonists. 29,32,61 CAMs act on assembly by priming dimers for assembly and increasing the amount of buried hydrophobic surface. 30,38,62 Some CAMs overfill the pocket and can drive the formation of aberrant particles and actually disrupt capsids. 30,38,44 With HBV, V124 normally forms part of one wall of the CAM pocket. We postulate the maleimidyl-BoDIPY modification overfills the pocket to favor disruption. To generalize, weak interactions are a requirement for the assembly of uniform capsids as they prevent trapping of misassembled subunits and support self-correction.⁶³ Likely, other virus capsids will have intersubunit weaknesses equivalent to the CAM site that cannot be overfilled without disrupting the global assembly. For example, the compound PF74 binds to hexamers of the HIV capsid protein and leads to capsid dissociation. 64-66

In the course of an in vivo viral infection, HBV capsid assembly and dissociation have thermodynamic, but not chemical, similarity to the strategy developed with Cp150-V124C—assembly, activation, and triggering (Figure 1). The full-length capsid protein includes the nucleic acid-binding 34 residues C-terminal domain (CTD), not present in Cp150-V124C. In vivo, capsid protein packages a linear, single-stranded viral RNA and a copy of the HBV polymerase, a thermodynamically favored reaction. In the RNA-filled capsid, the positive charge on the 240 CTDs (+16 charge per CTD, +3840/capsid) is approximately sufficient to neutralize the

charge of the viral RNA (-3200 plus a polyA tail). The resulting capsid is very stable. 36,67 Then, in the host, the RNA is reverse-transcribed to a circular dsDNA, a reaction where the RNA template is digested by the polymerase's RNaseH domain (nucleotides and digested RNA diffuse through the large pores in the capsid). The resulting DNA-filled capsid appears to be metastable, 36 "activated" in the parlance of Figure 1. The change in stability is probably due to the DNA's electrostatic repulsion and torsional stress. 37 The DNA-filled capsid packages about 3200 base pairs (-6400 charge) and dsDNA has a persistence length of about 50 nm compared to the inner diameter of 25 nm for a T=4 capsid. While purified capsids have been shown to be fragile, in vivo the triggering event is likely the interaction of the DNA-filled capsid with the machinery of the nuclear pore. 68

In the Cp150-V124C system, the mechanism of driving metastability by chemical modification is likely to require an understanding of quasi-equivalence and the potential for allosteric change. Even in HBV, a simple system, CAM sites are not equivalent and have distinct differences in molecular detail, and this heterogeneity may have an impact on the ability of C124 modification to drive dissociation. Structures of capsids show that bulky CAMs^{69–71} fit preferentially in the B and C pockets, which are capped by helix 5 from the C and D subunits, respectively. A model of the quasi-equivalent sites from a capsid—CAM complex⁷⁰ with a cysteine and maleimide modeled⁷² at position 124 in the capping helix emphasizes this difference (Figure 6). In the B and C pockets, in which the structure showed a CAM, there is plenty of room for modification of residue 124. In the A and D pockets,

modification of residue 124 (in helix 5 from the neighboring A and B subunits) will lead to collisions with the pocket (Figure 6 and see also Figure 4 in Schlicksup et al.²⁹). This observation suggests that modification of V124C from A and B subunits drives capsid destabilization. Nonetheless, we still need nearly 100% of the sites modified. This degree of modification suggests that there is a progressive accumulation of destabilizing energy over the capsid and that relaxing this energy by releasing dimers will influence subsequent pathways of capsid dissociation.

After dissociation is triggered, dissociation kinetics have several peculiarities. Foremost, there is a lag phase. A lag phase for a single crystal generally arises from a multibody reaction such as nucleation; 73,74 a capsid is an analogue to a single crystal. In an initial model, we have described a nucleation step for the release of subunits. This model may be general to other disassembly reactions and, indeed, may serve as part of the basis for HBV capsid's hysteresis to dissociation. ^{24,75} We also observe the appearance of intermediates between T = 4 capsid and 90-mer. This observation is consistent with percolation theory, 57,58 which posits that when a lattice incorporates enough flaws, it will catastrophically collapse. Percolation theory has been applied to HBV and generalized to other icosahedral symmetries. 57,58 Finally, at low β ME concentrations and low ionic strength, we observe the appearance of small oligomers of dimers (Figure 2C). We suspect that these small oligomers transiently accumulate because they are not forced into a capsid-like conformation, and thus, there is little driving force for their dissociation.

An advantage of using BoDIPY as a destabilizing agent is that we were able to observe dissociation by relaxation of self-FRET-induced depolarization of fluorescence. While at first this effect (low polarization for the large complex and high polarization for the free subunit) seemed counterintuitive, it is remarkably effective for demonstrating dissociation. ⁵⁰

We have reengineered the HBV capsid to be a redoxsensitive nanocontainer. Drawing on previous work, the Cp150-V124C dimer protein was assembled into extremely stable VLPs, which could be rendered metastable upon labeling with maleimidyl BoDIPY FL. While persistent in oxidizing conditions, a mild reducing agent like β ME in vitro or glutathione in hepatoma cells was sufficient to trigger complete dissociation. The general features observed with purified protein in vitro were also held in vivo. We have opened a door to programming dissociation into a VLP. There are specific areas where we emphasize the need to improve this technology. First, we need nearly 100% of the subunits to be modified to activate a capsid for dissociation. Second, in our model of dissociation, we have treated all subunits as equivalent instead of quasi-equivalent. These two areas may be closely related. We may need to consider methods to specifically label different quasi-equivalent interfaces. We also need to develop better intermolecular wedges (than maleimidyl BoDIPY FL) to trigger disassembly at lower levels of modification. Finally, we need to consider what other functions need to be programmed into a VLP to make it a better tool for delivering a cargo to a target.

ASSOCIATED CONTENT

Supporting Information

The Supporting Information is available free of charge at https://pubs.acs.org/doi/10.1021/jacs.2c10937.

Additional experimental methods, details, materials, and results (PDF)

AUTHOR INFORMATION

Corresponding Author

Adam Zlotnick — Molecular and Cellular Biochemistry, Indiana University, Bloomington, Indiana 47405, United States; orcid.org/0000-0001-9945-6267; Phone: (812) 856-1925; Email: azlotnic@indiana.edu

Authors

Caleb A. Starr — Molecular and Cellular Biochemistry, Indiana University, Bloomington, Indiana 47405, United States

 Smita Nair — Molecular and Cellular Biochemistry, Indiana University, Bloomington, Indiana 47405, United States;
Present Address: Door Pharmaceuticals, Bloomington, Indiana 47405, United States

Sheng-Yuan Huang – Department of Chemistry, Indiana University, Bloomington, Indiana 47405, United States

Michael F. Hagan — Martin Fisher School of Physics, Brandeis University, Waltham, Massachusetts 02454, United States; orcid.org/0000-0002-9211-2434

Stephen C. Jacobson — Department of Chemistry, Indiana University, Bloomington, Indiana 47405, United States; orcid.org/0000-0003-2415-041X

Complete contact information is available at: https://pubs.acs.org/10.1021/jacs.2c10937

Notes

The authors declare the following competing financial interest(s): A.Z. is on the Science advisory board for Assembly Biosciences. A.Z. is the founder and majority owner of Door Pharmaceuticals. Both of these are biotech start ups focused on antivirals. They represent no direct conflict and have had no effect on the data presented in this paper.

■ ACKNOWLEDGMENTS

This work was supported by NIH grants: R01 AI144022 to A.Z., R01 GM129354 and R35 GM141922 to S.C.J., and R01 GM108021 to M.F.H. This effort also used the Physical Biochemistry Instrumentation Facility and Electron Microscopy Center, supported by the Indiana Clinical and Translational Sciences Institute, and the Nanoscale Characterization Facility. M.F.H. also acknowledges the support of the Brandeis NSF MRSEC, Bioinspired Soft Materials, DMR-2011846. The authors thank Dr. Angela Patterson for her contributions.

REFERENCES

- (1) Ord, R. L.; Caldeira, J. C.; Rodriguez, M.; Noe, A.; Chackerian, B.; Peabody, D. S.; Gutierrez, G.; Lobo, C. A. A malaria vaccine candidate based on an epitope of the *Plasmodium falciparum* RHS protein. *Malar. J.* **2014**, *13*, No. 326.
- (2) Whitacre, D. C.; Espinosa, D. A.; Peters, C. J.; Jones, J. E.; Tucker, A. E.; Peterson, D. L.; Zavala, F. P.; Milich, D. R. *P. falciparum* and *P. vivax* Epitope-Focused VLPs Elicit Sterile Immunity to Blood Stage Infections. *PLoS One* **2015**, *10*, No. e0124856.
- (3) Pumpens, P.; Borisova, G. P.; Crowther, R. A.; Grens, E. Hepatitis B virus core particles as epitope carriers. *Intervirology* **1995**, 38, 63–74.
- (4) Pushko, P.; Pumpens, P.; Grens, E. Development of virus-like particle technology from small highly symmetric to large complex virus-like particle structures. *Intervirology* **2013**, *56*, 141–165.

- (5) Pumpens, P.; Renhofa, R.; Dishlers, A.; Kozlovska, T.; Ose, V.; Pushko, P.; Tars, K.; Grens, E.; Bachmann, M. F. The True Story and Advantages of RNA Phage Capsids as Nanotools. *Intervirology* **2016**, 59, 74–110.
- (6) Frietze, K. M.; Peabody, D. S.; Chackerian, B. Engineering virus-like particles as vaccine platforms. *Curr. Opin. Virol.* **2016**, *18*, 44–49.
- (7) Tao, P.; Zhu, J.; Mahalingam, M.; Batra, H.; Rao, V. B. Bacteriophage T4 nanoparticles for vaccine delivery against infectious diseases. *Adv. Drug Delivery Rev.* **2019**, *145*, 57–72.
- (8) Zamora-Ceballos, M.; Moreno, N.; Gil-Cantero, D.; Caston, J. R.; Blanco, E.; Barcena, J. Immunogenicity of Multi-Target Chimeric RHDV Virus-Like Particles Delivering Foreign B-Cell Epitopes. *Vaccines* **2022**, *10*, No. 229.
- (9) Chariou, P. L.; Ortega-Rivera, O. A.; Steinmetz, N. F. Nanocarriers for the Delivery of Medical, Veterinary, and Agricultural Active Ingredients. *ACS Nano* **2020**, *14*, 2678–2701.
- (10) Nkanga, C. I.; Steinmetz, N. F. The pharmacology of plant virus nanoparticles. *Virology* **2021**, *556*, 39–61.
- (11) Desjardins, A.; Gromeier, M.; Herndon, J. E., 2nd; Beaubier, N.; Bolognesi, D. P.; Friedman, A. H.; Friedman, H. S.; McSherry, F.; Muscat, A. M.; Nair, S.; Peters, K. B.; Randazzo, D.; Sampson, J. H.; Vlahovic, G.; Harrison, W. T.; McLendon, R. E.; Ashley, D.; Bigner, D. D. Recurrent Glioblastoma Treated with Recombinant Poliovirus. N. Engl. J. Med. 2018, 379, 150–161.
- (12) Lucon, J.; Qazi, S.; Uchida, M.; Bedwell, G. J.; LaFrance, B.; Prevelige, P. E., Jr.; Douglas, T. Use of the interior cavity of the P22 capsid for site-specific initiation of atom-transfer radical polymerization with high-density cargo loading. *Nat. Chem.* **2012**, *4*, 781–788.
- (13) McCoy, K.; Selivanovitch, E.; Luque, D.; Lee, B.; Edwards, E.; Caston, J. R.; Douglas, T. Cargo Retention inside P22 Virus-Like Particles. *Biomacromolecules* **2018**, *19*, 3738–3746.
- (14) Waghwani, H. K.; Uchida, M.; Fu, C. Y.; LaFrance, B.; Sharma, J.; McCoy, K.; Douglas, T. Virus-Like Particles (VLPs) as a Platform for Hierarchical Compartmentalization. *Biomacromolecules* **2020**, *21*, 2060–2072.
- (15) Dragnea, B. Bio-inspired materials: unnatural life. *Nat. Mater.* **2008**, *7*, 102–104.
- (16) Cheng, F.; Tsvetkova, I. B.; Khuong, Y. L.; Moore, A. W.; Arnold, R. J.; Goicochea, N. L.; Dragnea, B.; Mukhopadhyay, S. The packaging of different cargo into enveloped viral nanoparticles. *Mol Pharm.* 2013, 10, 51–58.
- (17) Sun, J.; DuFort, C.; Daniel, M. C.; Murali, A.; Chen, C.; Gopinath, K.; Stein, B.; De, M.; Rotello, V. M.; Holzenburg, A.; Kao, C. C.; Dragnea, B. Core-controlled polymorphism in virus-like particles. *Proc. Natl. Acad. Sci. U.S.A.* **2007**, *104*, 1354–1359.
- (18) Bode, S. A.; Minten, I. J.; Nolte, R. J.; Cornelissen, J. J. Reactions inside nanoscale protein cages. *Nanoscale* **2011**, *3*, 2376–2389
- (19) Brasch, M.; Putri, R. M.; de Ruiter, M. V.; Luque, D.; Koay, M. S.; Caston, J. R.; Cornelissen, J. J. Assembling Enzymatic Cascade Pathways inside Virus-Based Nanocages Using Dual-Tasking Nucleic Acid Tags. J. Am. Chem. Soc. 2017, 139, 1512—1519.
- (20) Llauró, A.; Luque, D.; Edwards, E.; Trus, B. L.; Avera, J.; Reguera, D.; Douglas, T.; Pablo, P. J.; Caston, J. R. Cargo-shell and cargo-cargo couplings govern the mechanics of artificially loaded virus-derived cages. *Nanoscale* **2016**, *8*, 9328–9336.
- (21) Vogel, M.; Vorreiter, J.; Nassal, M. Quaternary structure is critical for protein display on capsid-like particles (CLPs): efficient generation of hepatitis B virus CLPs presenting monomeric but not dimeric and tetrameric fluorescent proteins. *Proteins* **2004**, *58*, 478–488.
- (22) Heger-Stevic, J.; Kolb, P.; Walker, A.; Nassal, M. Displaying Whole-Chain Proteins on Hepatitis B Virus Capsid-Like Particles. *Methods Mol. Biol.* **2018**, *1776*, 503–31.
- (23) Wu, W.; Watts, N. R.; Cheng, N.; Huang, R.; Steven, A. C.; Wingfield, P. T. Expression of quasi-equivalence and capsid dimorphism in the Hepadnaviridae. *PLoS Comput Biol* **2020**, *16*, No. e1007782.

- (24) Starr, C. A.; Barnes, L. F.; Jarrold, M. F.; Zlotnick, A. Hysteresis in Hepatitis B Virus (HBV) Requires Assembly of Near-Perfect Capsids. *Biochemistry* **2022**, *61*, 505–513.
- (25) Harms, Z. D.; Selzer, L.; Zlotnick, A.; Jacobson, S. C. Monitoring Assembly of Virus Capsids with Nanofluidic Devices. *ACS Nano* **2015**, *9*, 9087–9096.
- (26) Lutomski, C. A.; Lyktey, N. A.; Pierson, E. E.; Zhao, Z.; Zlotnick, A.; Jarrold, M. F. Multiple Pathways in Capsid Assembly. *J. Am. Chem. Soc.* **2018**, *140*, 5784–5790.
- (27) Asor, R.; Schlicksup, C. J.; Zhao, Z.; Zlotnick, A.; Raviv, U. Rapidly Forming Early Intermediate Structures Dictate the Pathway of Capsid Assembly. J. Am. Chem. Soc. 2020, 142, 7868–7882.
- (28) Mohajerani, F.; Tyukodi, B.; Schlicksup, C. J.; Hadden-Perilla, J. A.; Zlotnick, A.; Hagan, M. F. Multiscale Modeling of Hepatitis B Virus Capsid Assembly and Its Dimorphism. *ACS Nano* **2022**, *16*, 13845–13859.
- (29) Schlicksup, C. J.; Zlotnick, A. Viral structural proteins as targets for antivirals. *Curr. Opin. Virol.* **2020**, *45*, 43–50.
- (30) Berke, J. M.; Dehertogh, P.; Vergauwen, K.; Mostmans, W.; Vandyck, K.; Raboisson, P.; Pauwels, F. Antiviral Properties and Mechanism of Action Studies of the Hepatitis B Virus Capsid Assembly Modulator JNJ-56136379. *Antimicrob. Agents Chemother.* **2020**, *64*, No. e02439-19.
- (31) Kim, H.; Ko, C.; Lee, J. Y.; Kim, M. Current Progress in the Development of Hepatitis B Virus Capsid Assembly Modulators: Chemical Structure, Mode-of-Action and Efficacy. *Molecules* **2021**, *26*, No. 7420.
- (32) Niklasch, M.; Zimmermann, P.; Nassal, M. The Hepatitis B Virus Nucleocapsid-Dynamic Compartment for Infectious Virus Production and New Antiviral Target. *Biomedicines* **2021**, *9*, No. 1577.
- (33) Tsounis, E. P.; Tourkochristou, E.; Mouzaki, A.; Triantos, C. Toward a new era of hepatitis B virus therapeutics: The pursuit of a functional cure. *World J. Gastroenterol.* **2021**, *27*, 2727–2757.
- (34) Wingfield, P. T.; Stahl, S. J.; Williams, R. W.; Steven, A. C. Hepatitis core antigen produced in *Escherichia coli*: subunit composition, conformational analysis, and in vitro capsid assembly. *Biochemistry* **1995**, *34*, 4919–4932.
- (35) Uetrecht, C.; Watts, N. R.; Stahl, S. J.; Wingfield, P. T.; Steven, A. C.; Heck, A. J. Subunit exchange rates in Hepatitis B virus capsids are geometry- and temperature-dependent. *Phys. Chem. Chem. Phys* **2010**, *12*, 13368–13371.
- (36) Cui, X.; Ludgate, L.; Ning, X.; Hu, J. Maturation-associated destabilization of hepatitis B virus nucleocapsid. *J. Virol.* **2013**, *87*, 11494–11503.
- (37) Dhason, M. S.; Wang, J. C.; Hagan, M. F.; Zlotnick, A. Differential assembly of Hepatitis B Virus core protein on single- and double-stranded nucleic acid suggest the dsDNA-filled core is springloaded. *Virology* **2012**, 430, 20–29.
- (38) Berke, J. M.; Dehertogh, P.; Vergauwen, K.; Van Damme, E.; Mostmans, W.; Vandyck, K.; Pauwels, F. Capsid Assembly Modulators Have a Dual Mechanism of Action in Primary Human Hepatocytes Infected with Hepatitis B Virus. *Antimicrob. Agents Chemother.* **2017**, *61*, No. e00560-17.
- (39) WHO. Global Hepatitis Report, World Health Organization 2017.
- (40) Zoulim, F.; Zlotnick, A.; Buchholz, S.; Donaldson, E.; Fry, J.; Gaggar, A.; Hu, J.; Kann, M.; Lenz, O.; Lin, K.; Nagraj, N.; Nassal, M.; Delaney, W. E. I.; Wang, S.; Westman, G.; Miller, V.; Janssen, H. L. A. Nomenclature of HBV core protein targeting antivirals. *Nat. Gastroenterol. Hepatol.* **2022**, *19*, 748–750.
- (41) Katen, S. P.; Chirapu, S. R.; Finn, M. G.; Zlotnick, A. Trapping of Hepatitis B Virus capsid assembly intermediates by phenyl-propenamide assembly accelerators. *ACS Chem Biol* **2010**, *5*, 1125–1136
- (42) Bourne, C.; Finn, M. G.; Zlotnick, A. Global structural changes in hepatitis B capsids induced by the assembly effector HAP1. *J. Virol.* **2006**, *80*, 11055–11061.
- (43) Zhou, Z.; Hu, T.; Zhou, X.; Wildum, S.; Garcia-Alcalde, F.; Xu, Z.; Wu, D.; Mao, Y.; Tian, X.; Zhou, Y.; Shen, F.; Zhang, Z.; Tang, G.;

- Najera, I.; Yang, G.; Shen, H. C.; Young, J. A.; Qin, N. Heteroaryldihydropyrimidine (HAP) and Sulfamoylbenzamide (SBA) Inhibit Hepatitis B Virus Replication by Different Molecular Mechanisms. *Sci. Rep.* **2017**, *7*, No. 42374.
- (44) Schlicksup, C. J.; Laughlin, P.; Dunkelbarger, S.; Wang, J. C.; Zlotnick, A. Local Stabilization of Subunit-Subunit Contacts Causes Global Destabilization of Hepatitis B Virus Capsids. *ACS Chem. Biol.* **2020**, *15*, 1708–1717.
- (45) Zhao, Z.; Wang, J. C.; Segura, C. P.; Hadden-Perilla, J. A.; Zlotnick, A. The Integrity of the Intradimer Interface of the Hepatitis B Virus Capsid Protein Dimer Regulates Capsid Self-Assembly. *ACS Chem. Biol.* **2020**, *15*, 3124–3132.
- (46) Lee, L. S.; Brunk, N.; Haywood, D. G.; Keifer, D.; Pierson, E.; Kondylis, P.; Wang, J. C.; Jacobson, S. C.; Jarrold, M. F.; Zlotnick, A. A molecular breadboard: Removal and replacement of subunits in a hepatitis B virus capsid. *Protein Sci.* **2017**, *26*, 2170–2180.
- (47) Zlotnick, A.; Lee, A.; Bourne, C. R.; Johnson, J. M.; Domanico, P. L.; Stray, S. J. In vitro screening for molecules that affect virus capsid assembly (and other protein association reactions). *Nat. Protoc.* **2007**, *2*, 490–498.
- (48) Harms, Z. D.; Haywood, D. G.; Kneller, A. R.; Selzer, L.; Zlotnick, A.; Jacobson, S. C. Single-particle electrophoresis in nanochannels. *Anal. Chem.* **2015**, *87*, 699–705.
- (49) Qazi, S.; Schlicksup, C. J.; Rittichier, J.; VanNieuwenhze, M. S.; Zlotnick, A. An Assembly-Activating Site in the Hepatitis B Virus Capsid Protein Can Also Trigger Disassembly. *ACS Chem. Biol.* **2018**, 13, 2114–2120.
- (50) Chan, F. T. S.; Kaminski, C. F.; Kaminski Schierle, G. S. HomoFRET fluorescence anisotropy imaging as a tool to study molecular self-assembly in live cells. *ChemPhysChem* **2011**, *12*, 500–509.
- (51) Ceres, P.; Zlotnick, A. Weak protein-protein interactions are sufficient to drive assembly of hepatitis B virus capsids. *Biochemistry* **2002**, *41*, 11525–11531.
- (52) Zhao, Z.; Wang, J. C.; Gonzalez-Gutierrez, G.; Venkatakrishnan, B.; Asor, R.; Khaykelson, D.; Raviv, U.; Zlotnick, A. Structural Differences between the Woodchuck Hepatitis Virus Core Protein in the Dimer and Capsid States Are Consistent with Entropic and Conformational Regulation of Assembly. *J. Virol.* **2019**, 93, No. e00141-19.
- (53) Kegel, W. K.; van der Schoot, P. Competing hydrophobic and screened-coulomb interactions in hepatitis B virus capsid assembly. *Biophys. J.* **2004**, *86*, 3905–3913.
- (54) Kondylis, P.; Schlicksup, C. J.; Zlotnick, A.; Jacobson, S. C. Analytical Techniques to Characterize the Structure, Properties, and Assembly of Virus Capsids. *Anal. Chem.* **2019**, *91*, 622–636.
- (55) Zhou, J.; Kondylis, P.; Haywood, D. G.; Harms, Z. D.; Lee, L. S.; Zlotnick, A.; Jacobson, S. C. Characterization of Virus Capsids and Their Assembly Intermediates by Multicycle Resistive-Pulse Sensing with Four Pores in Series. *Anal. Chem.* **2018**, *90*, 7267–7274.
- (56) Zhou, J.; Zlotnick, A.; Jacobson, S. C. Disassembly of Single Virus Capsids Monitored in Real Time with Multicycle Resistive-Pulse Sensing. *Anal. Chem.* **2022**, *94*, 985–992.
- (57) Brunk, N. E.; Lee, L. S.; Glazier, J. A.; Butske, W. D.; Zlotnick, A. Molecular Jenga: The Percolation Phase Transition (Collapse) in Virus Capsids. *Phys Biol* **2018**, *15*, No. 056005.
- (58) Brunk, N. E.; Twarock, R. Percolation Theory Reveals Biophysical Properties of Virus-like Particles. *ACS Nano* **2021**, *15*, 12988–95.
- (59) Forman, H. J.; Zhang, H.; Rinna, A. Glutathione: overview of its protective roles, measurement, and biosynthesis. *Mol. Aspects Med.* **2009**, *30*, 1–12.
- (60) Conway, J. F.; Watts, N. R.; Belnap, D. M.; Cheng, N.; Stahl, S. J.; Wingfield, P. T.; Steven, A. C. Characterization of a conformational epitope on hepatitis B virus core antigen and quasiequivalent variations in antibody binding. *J. Virol.* **2003**, *77*, 6466–6473.
- (61) Alter, H.; Block, T.; Brown, N.; Brownstein, A.; Brosgart, C.; Chang, K. M.; Chen, P. J.; Chisari, F. V.; Cohen, C.; El-Serag, H.; Feld, J.; Gish, R.; Glenn, J.; Greten, T.; Guo, H.; Guo, J. T.; Hoshida,

- Y.; Hu, J.; Kowdley, K. V.; Li, W.; Liang, J.; Locarnini, S.; Lok, A. S.; Mason, W.; McMahon, B.; Mehta, A.; Perrillo, R.; Revill, P.; Rice, C. M.; Rinaudo, J.; Schinazi, R.; Seeger, C.; Shetty, K.; Tavis, J.; Zoulim, F. A research agenda for curing chronic hepatitis B virus infection. *Hepatology* **2018**, *67*, 1127–1131.
- (62) Stray, S. J.; Bourne, C. R.; Punna, S.; Lewis, W. G.; Finn, M. G.; Zlotnick, A. A heteroaryldihydropyrimidine activates and can misdirect hepatitis B virus capsid assembly. *Proc. Natl. Acad. Sci. U.S.A.* 2005, 102, 8138–8143.
- (63) Katen, S. P.; Zlotnick, A. Thermodynamics of Virus Capsid Assembly. *Methods Enzymol.* **2009**, 455, 395–417.
- (64) Bhattacharya, A.; Alam, S. L.; Fricke, T.; Zadrozny, K.; Sedzicki, J.; Taylor, A. B.; Demeler, B.; Pornillos, O.; Ganser-Pornillos, B. K.; Diaz-Griffero, F.; Ivanov, D. N.; Yeager, M. Structural basis of HIV-1 capsid recognition by PF74 and CPSF6. *Proc. Natl. Acad. Sci. U.S.A.* **2014**, *111*, 18625–18630.
- (65) McArthur, C.; Gallazzi, F.; Quinn, T. P.; Singh, K. HIV Capsid Inhibitors Beyond PF74. *Diseases* **2019**, *7*, No. 56.
- (66) Shi, J.; Zhou, J.; Shah, V. B.; Aiken, C.; Whitby, K. Small-molecule inhibition of human immunodeficiency virus type 1 infection by virus capsid destabilization. *J. Virol.* **2011**, *85*, 542–549.
- (67) Porterfield, J. Z.; Dhason, M. S.; Loeb, D. D.; Nassal, M.; Stray, S. J.; Zlotnick, A. Full-Length Hepatitis B Virus Core Protein Packages Viral and Heterologous RNA with Similarly High Levels of Cooperativity. *J. Virol.* **2010**, *84*, 7174–7184.
- (68) Gallucci, L.; Kann, M. Nuclear Import of Hepatitis B Virus Capsids and Genome. *Viruses* **2017**, *9*, No. 21.
- (69) Katen, S. P.; Tan, Z.; Chirapu, S. R.; Finn, M. G.; Zlotnick, A. Assembly-directed antivirals differentially bind quasiequivalent pockets to modify hepatitis B virus capsid tertiary and quaternary structure. *Structure* **2013**, *21*, 1406–1416.
- (70) Schlicksup, C. J.; Wang, J. C.; Francis, S.; Venkatakrishnan, B.; Turner, W. W.; VanNieuwenhze, M.; Zlotnick, A. Hepatitis B virus core protein allosteric modulators can distort and disrupt intact capsids. *eLife* **2018**, *7*, No. e31473.
- (71) Venkatakrishnan, B.; Katen, S. P.; Francis, S.; Chirapu, S.; Finn, M. G.; Zlotnick, A. Hepatitis B Virus Capsids Have Diverse Structural Responses to Small-Molecule Ligands Bound to the Heteroaryldihydropyrimidine Pocket. *J. Virol.* **2016**, *90*, 3994–4004.
- (72) Goddard, T. D.; Huang, C. C.; Meng, E. C.; Pettersen, E. F.; Couch, G. S.; Morris, J. H.; Ferrin, T. E. UCSF ChimeraX: Meeting modern challenges in visualization and analysis. *Protein Sci.* **2018**, 27, 14–25.
- (73) Timmermans, S. B. P. E.; Ramezani, A.; Montalvo, T.; Nguyen, M.; van der Schoot, P.; van Hest, J. C. M.; Zandi, R. The Dynamics of Viruslike Capsid Assembly and Disassembly. *J. Am. Chem. Soc.* **2022**, 144, 12608–12612.
- (74) van der Schoot, P.; Zandi, R. Kinetic theory of virus capsid assembly. *Phys. Biol.* **2007**, *4*, 296–304.
- (75) Singh, S.; Zlotnick, A. Observed hysteresis of virus capsid disassembly is implicit in kinetic models of assembly. *J. Biol. Chem.* **2003**, 278, 18249–18255.